Ternary Hybrid Nanoparticle Isomers: Directing the Nucleation of Ag on Pt−Fe_3O_4 Using a Solid-State Protecting Group

James M. Hodges, Adam J. Biacchi, and Raymond E. Schaak*

Department of Chemistry and Materials Research Institute, The Pennsylvania State University, University Park, Pennsylvania 16802, United States

ABSTRACT Colloidal hybrid nanoparticles are an important class of materials that incorporate multiple nanoparticles into a single system through solid-state interfaces, which can result in multifunctionality and the emergence of synergistic properties not found in the individual components. These hybrid structures are typically produced using seeded-growth methods, where preformed nanoparticles serve as seeds onto which additional domains are added through subsequent reactions. For hybrid nanoparticles that contain more than two domains, multiple configurations with distinct connectivities and functionalities are possible, and these can be considered as nanoparticle analogues of molecular isomers. However, accessing one isomer relative to others in the same hybrid nanoparticle system is challenging, particularly when the formation of a target isomer is disfavored relative to more stable or synthetically accessible configurations. Here, we show that an iron oxide shell installed onto the Pt domain of Pt−Fe_3O_4 hybrid nanoparticles serves as a solid-state protecting group that can direct the nucleation of a third domain to an otherwise disfavored site. Under traditional conditions, Ag nucleates exclusively onto the Pt domain of Pt−Fe_3O_4 heterodimers, resulting in the formation of the Ag−Pt−Fe_3O_4 heterotrimer isomer. When the Pt surface is covered with an iron oxide protecting group, the nucleation of Ag is redirected onto the Fe_3O_4 domain, producing the distinct and otherwise inaccessible Pt−Fe_3O_4−Ag isomer. Similar results are obtained for the Au−Pt−Fe_3O_4 system, where formation of the favored Au−Pt−Fe_3O_4 configuration is blocked by the iron oxide protecting group. The thickness of the iron oxide shell that protects the Pt domain can be systematically tuned by adjusting the ratio of oleic acid to iron pentacarbonyl during the synthesis of the Pt−Fe_3O_4 heterodimers, and this insight is important for controllably implementing the protecting group chemistry.

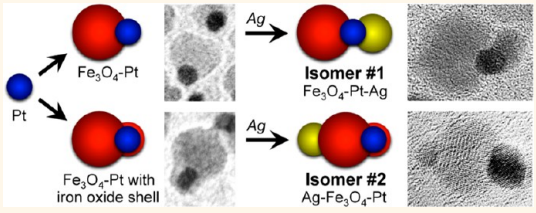

KEYWORDS: colloidal hybrid nanoparticles · nanoparticle synthesis · nanocrystals · Pt−Fe_3O_4 · heterodimers · heterotrimers · seeded growth · protecting group · nanoparticle isomers

Colloidal hybrid nanoparticles integrate multiple nanoscale domains into one system that can exhibit properties not found in the individual components. These synergistic qualities are a result of electronic and magnetic communication at the solid-state heterojunctions within these structures.[1−9] At the nanoscale, these interfacial properties are not always confined to the domain boundary and can pervade throughout the material, resulting in properties not attainable in the bulk. Additionally, careful arrangement of constituent domains can lead to cooperative processes within the particles that facilitate enhanced functionality.[10,11] For these reasons, hybrid nanomaterials are excellent candidates for applications in solar energy conversion,[12,13] heterogeneous catalysis,[14,15] magnetism,[16] electronics,[17] and biomedical imaging.[18]

Although numerous methods have been demonstrated to be effective for producing hybrid nanoparticles, the multistep seeded growth approach is among the most common due to its versatility in a wide variety of systems.[10,19−21] In this strategy, preformed nanocrystals are used as seeds for adding additional domains, in a stepwise manner, through subsequent reactions.[21] As the applications of hybrid nanoparticles continue to expand and become more sophisticated, their materials requirements are becoming more explicit and rigid, particularly with respect to the types and sequences of materials linkages in higher-order systems containing more than two domains. Using

* Address correspondence to schaak@chem.psu.edu.

Received for review November 16, 2013 and accepted December 13, 2013.

Published online December 13, 2013
10.1021/nn405943z

an arbitrary nanoparticle heterotrimer as an example, the nucleation of a third domain (C) onto a preformed A–B heterodimer could lead to several distinct configurations, including A–B–C and C–A–B linkages. These distinct configurations, A–B–C and C–A–B, can be considered as nanoparticle analogues of molecular isomers, because each contains the same materials but with distinct connectivities and consequently different functionalities.

Controlling such domain arrangements in hybrid nanoparticle systems is important across a wide range of applications. For example, photocatalytic water splitting can be enabled by specific configurations of semiconducting and metal nanoparticles that are designed to absorb incident photons and convert them into separated electron–hole pairs.[22] The necessary interfacial electron transfer processes are best facilitated by one particular sequence of material linkages, and therefore efficiency is greatest when the yield of the desired configuration is maximized, since other configurations are less active or inactive. Likewise, specific domain arrangements in optical heterostructures can modulate changes in absorbance and emission phenomena. For example, the photoluminescence efficiency of CdS quantum dots is increased when they are in close proximity to plasmonic nanoparticles,[23,24] but emission can be quenched when there is direct contact.[25] Since the relative locations of nanoparticle domains define the connectivity and consequent functionality of a hybrid nanoparticle, synthetic tools that permit site-specific nucleation and that provide access to the targeted configurations in high yields are therefore essential.[26]

As a route to colloidal hybrid nanoparticles, heterogeneous seeded nucleation is typically either nonselective, resulting in overgrowth on all domains, or highly selective, resulting in the exclusive formation of one specific isomer relative to others that may be preferred for a particular application. For example, Ag has been shown to nucleate only on the Pt domain of Pt–Fe_3O_4 hybrid nanoparticles, forming exclusively the Ag–Pt–Fe_3O_4 isomer (rather than, for example, Pt–Fe_3O_4–Ag) despite the accessibility of the Fe_3O_4 surface and the known affinity of Ag to also nucleate on Fe_3O_4 nanoparticles.[21] For molecules, one can often direct reactivity to one particular functional group when multiple ones are accessible by installing a protecting group to block access to the undesired location while leaving the desired functional group exposed. A nanoparticle analogue of molecular protecting group chemistry would be a powerful addition to the "total synthesis toolbox"[21,27] for constructing high-order colloidal hybrid nanoparticles controllably and in high yield.

Accordingly, here we provide a proof-of-concept demonstration, for a model system, that a thin amorphous iron oxide shell can serve as a solid-state protecting group in colloidal hybrid nanoparticles to facilitate controllable regioselective nucleation and the predictable formation of distinct ternary (heterotrimer) isomers. Specifically, we show that both Ag–Pt–Fe_3O_4 and Pt–Fe_3O_4–Ag can be accessed in high yield by directing the nucleation of Ag nanoparticles selectively to either the Pt or Fe_3O_4 domains of Pt–Fe_3O_4 heterodimers. The propensity for Ag to nucleate on the Pt domain of Pt–Fe_3O_4 can be overcome by growing a thin amorphous iron oxide shell on the Pt domain as a protecting group, effectively blocking the Pt surface. This results in the nucleation of Ag on the Fe_3O_4 domain, forming the otherwise disfavored Pt–Fe_3O_4–Ag isomer. The iron oxide protecting group also blocks the Pt domain from nucleating other nanoparticles, such as Au. Finally, in-depth investigations into the reaction conditions that lead to the formation of the iron oxide shell provide detailed guidelines for reproducibly applying this solid-state protecting group to hybrid nanoparticle systems.

RESULTS AND DISCUSSION

Selective Synthesis of Ag–Pt–Fe_3O_4 and Pt–Fe_3O_4–Ag Hybrid Nanoparticle Isomers. Pt–Fe_3O_4 heterodimers were synthesized by decomposing $Fe(CO)_5$ in the presence of Pt seeds, as described previously.[28] A representative TEM image of the resulting Pt–Fe_3O_4 heterodimers is shown in Figure 1a, along with a STEM-EDS line scan (Figure 1b) showing the distribution of Pt and Fe (*via* the Pt M-shell and Fe K-shell transitions) across a representative Pt–Fe_3O_4 heterodimer. Both Fe and Pt are present at the Pt–Fe_3O_4 interface (because Fe_3O_4 partially envelopes the Pt domain), but the Fe signal decreases rapidly as the Pt signal increases, with near-baseline Fe signal at the outer edge of the Pt domain.

As a control experiment, when the Pt–Fe_3O_4 heterodimers from Figure 1a react with $Ag(C_2H_3O_2)$ in toluene at 60 °C, Ag nanoparticles nucleate exclusively on the Pt domain to form Ag–Pt–Fe_3O_4 heterotrimers.[21] A representative TEM image of the Ag–Pt–Fe_3O_4 heterotrimers is shown in Figure 1c, along with a HRTEM image of a single Ag–Pt–Fe_3O_4 heterotrimer in Figure 1e. The observed lattice spacings are 2.3, 2.0, and 4.9 Å, which are consistent with the (111) plane of Ag, the (100) plane of Pt, and the (111) plane of Fe_3O_4, respectively. The STEM-EDS element mapping data in Figure 1d further confirms the formation of an Ag–Pt–Fe_3O_4 heterotrimer, based on comparing the spatial distribution of the Ag L-shell, Pt M-shell, and Fe K-shell transitions with the corresponding STEM image in the inset.

Taken together, these data confirm that the Pt domains of as-synthesized Pt–Fe_3O_4 heterodimers are active and selective toward nucleation of Ag to form exclusively Ag–Pt–Fe_3O_4 heterotrimers. However, in order to access other isomers, the reactivity of the Pt domain must be blocked so that only the

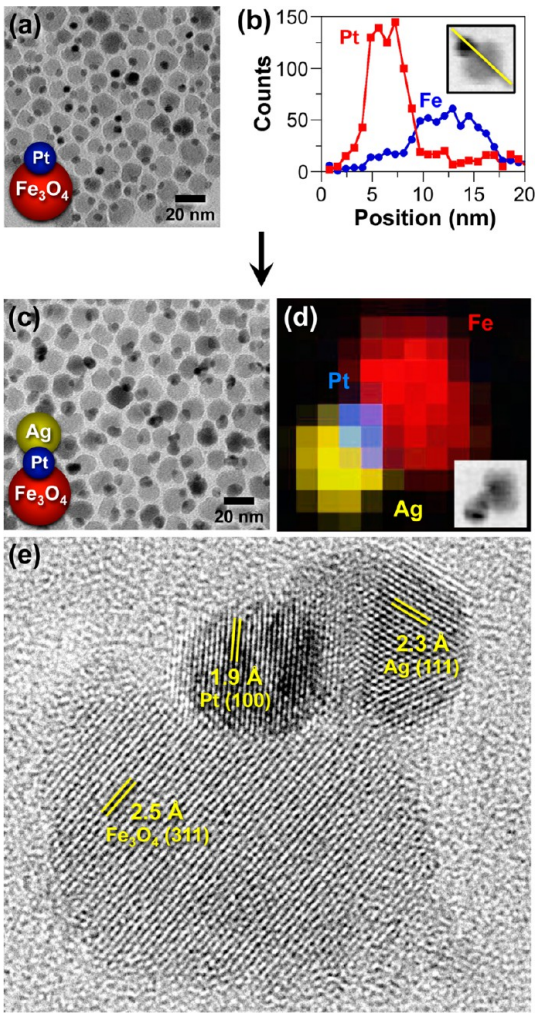

Figure 1. (a) TEM image of Pt−Fe_3O_4 heterodimer seeds and (b) STEM-EDS line scan of a typical Pt−Fe_3O_4 heterodimer, showing the distribution of Fe and Pt across the hybrid particle. (c) Representative TEM image of Ag−Pt−Fe_3O_4 heterotrimers, which form from the nucleation of Ag on the Pt−Fe_3O_4 heterodimers shown in (a). (d) Composite STEM-EDS element map of an individual Ag−Pt−Fe_3O_4 heterotrimer particle (corresponding STEM image shown in the inset) that includes an overlay of the Ag L-shell (yellow), Pt M-shell (blue), and Fe K-shell (red) transitions. (e) HRTEM image of a representative Ag−Pt−Fe_3O_4 heterotrimer, highlighting lattice spacings that are characteristic of Fe_3O_4, Pt, and Ag.

Fe_3O_4 surface is exposed and capable of nucleating Ag. Under identical reaction conditions, Ag is known to nucleate on both Fe_3O_4 and Pt nanoparticle surfaces when the Fe_3O_4 and Pt nanoparticles are isolated from one another, *e.g.*, when they are not connected as hybrid nanoparticles, and this capability helped to motivate our choice of Ag/Pt/Fe_3O_4 as a model system for proof-of-concept studies.[21] Ag therefore also has an affinity for the Fe_3O_4 surface, which suggests that if the Pt surface is blocked and only the Fe_3O_4 surface is accessible, Ag may nucleate on Fe_3O_4 instead of Pt to produce a distinct isomer, Ag−Fe_3O_4−Pt. Chemistry similar to that used to synthesize the Pt−Fe_3O_4 heterodimers—reaction of Au seeds with $Fe(CO)_5$ in

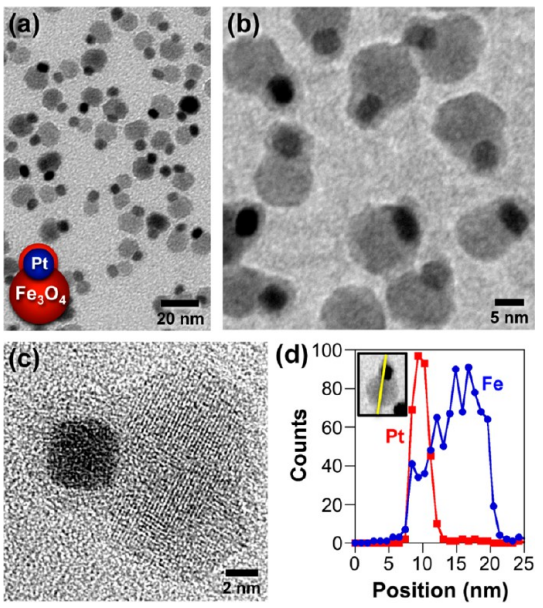

Figure 2. (a, b) Representative TEM images, at two different magnifications, of Pt−Fe_3O_4 heterodimers that contain an amorphous iron oxide shell surrounding the Pt domain. (c) HRTEM image of a single Pt−Fe_3O_4 heterodimer containing an iron oxide shell, showing that the Fe_3O_4 domain is crystalline and the shell surrounding the Pt domain is amorphous. (d) STEM-EDS line scan of a Pt−Fe_3O_4 heterodimer containing an iron oxide shell, showing the distribution of Fe and Pt across the particle.

1-octadecene—has been used to make Au−Fe_3O_4 heterodimers with a thin iron oxide shell surrounding the Au domain.[28] This suggests that it may be possible to install a thin iron oxide shell on the Pt surface of the Pt−Fe_3O_4 heterodimers in order to block access to Pt and instead direct nucleation of Ag onto the Fe_3O_4 surface.

We found that a key and highly reproducible experimental variable for coating the Pt domain with an iron oxide shell is through careful adjustment of the molar ratio of oleic acid to $Fe(CO)_5$. Specifically, when the molar ratio of oleic acid to $Fe(CO)_5$ is reduced from the typical value of 3:1[28] to 1.5:1, the resulting Pt−Fe_3O_4 heterodimers exhibit a thin oxide shell on the Pt domain. A representative TEM image (Figure 2a) shows Pt−Fe_3O_4 heterodimers that, at low magnification, look identical to those shown in Figure 1a. However, a higher-magnification image (Figure 2b) reveals that there are shells around the Pt domains, and this is confirmed by the HRTEM image in Figure 2c. The HRTEM image in Figure 2c also indicates that the iron oxide shell that surrounds the Pt domain is amorphous. A STEM-EDS line scan (Figure 2d) shows the distribution of Pt and Fe across a corresponding Pt−Fe_3O_4 heterodimer. In comparison with the STEM-EDS line scan in Figure 1b for the Pt−Fe_3O_4 heterodimer with no shell, where the Fe signal approaches baseline toward the edge of the Pt domain, the Fe signal persists across the Pt domain, including at its edge. This is consistent with the presence of an iron oxide shell

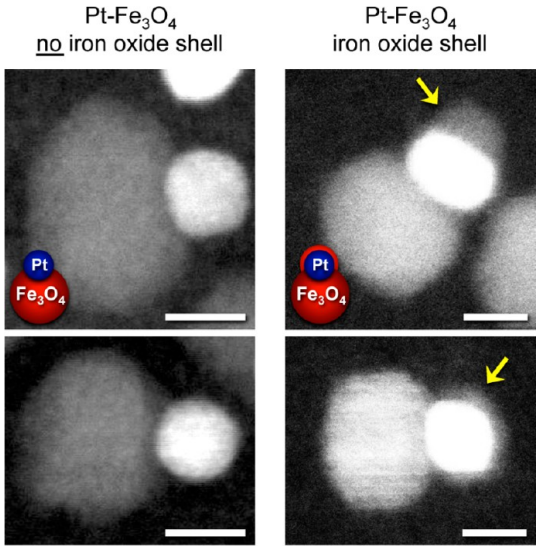

Figure 3. HAADF STEM images of (left) Pt−Fe_3O_4 heterodimers and (right) Pt−Fe_3O_4 heterodimers that contain an iron oxide shell surrounding the Pt domain. All scale bars are 5 nm.

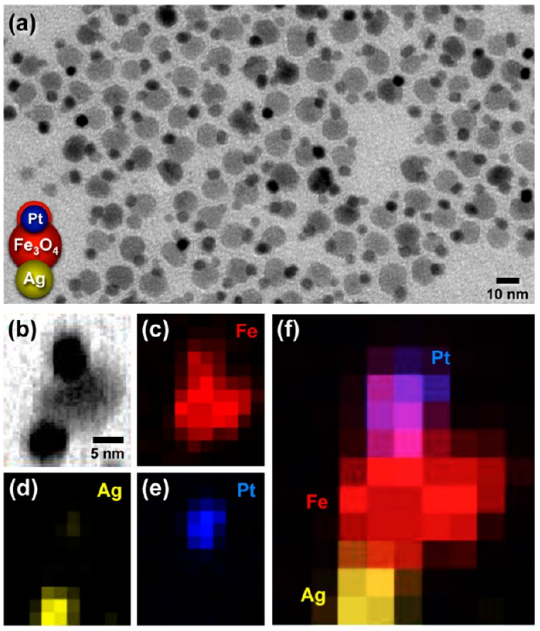

Figure 4. (a) Representative TEM image of Pt−Fe_3O_4−Ag heterotrimers. (b) STEM image and corresponding element maps for the (c) Fe K-shell, (d) Ag L-shell, and (e) Pt M-shell transitions. A composite STEM-EDS element map, including an overlay of the Ag (yellow), Pt (blue), and Fe (red) element maps from (c)−(e), is shown in (f). The Pt domain appears purple in the composite image in (f) because the Pt is covered by a shell of iron oxide and therefore the Pt (blue) and Fe (red) signals overlap.

surrounding the Pt domain. Further support of an iron oxide shell is provided by the HAADF-STEM images in Figure 3, which clearly show that shells of similar Z-contrast to those of the Fe_3O_4 regions surround the Pt particles in Pt−Fe_3O_4 heterodimers that were prepared with a 1.5:1 ratio of oleic acid to $Fe(CO)_5$. For comparison, no such shell is observed in the HAADF-STEM images of the Pt−Fe_3O_4 heterodimers prepared using the traditional 3:1 ratio of oleic acid to $Fe(CO)_5$. Collectively, the data indicate that decreasing the oleic acid concentration relative to that of $Fe(CO)_5$ leads to the growth of an iron oxide shell that coats the surface of the Pt domain.

While the reaction of the Pt−Fe_3O_4 heterodimers from Figure 1a with $Ag(C_2H_3O_2)$ in toluene at 60 °C led exclusively to the formation of Ag−Pt−Fe_3O_4 heterotrimers (Figure 1c), the reaction under the same conditions but instead using the Pt−Fe_3O_4 heterodimers from Figure 2—which contain a thin iron oxide shell surrounding the Pt domain—does not result in nucleation of Ag on Pt, but rather exclusively on Fe_3O_4. Figure 4a shows a representative TEM image of the Pt−Fe_3O_4−Ag heterotrimers. Figure 4b−f show STEM-EDS element mapping data that confirm the spatial distribution of Ag, Pt, and Fe in a representative Pt−Fe_3O_4−Ag heterotrimer. Closer inspection of the TEM image in Figure 4a reveals that 85% of the sample consists of heterotrimer products with three distinct morphologies, and 15% of the sample consists of non-heterotrimer impurities (*e.g.*, Pt−Fe_3O_4, Pt, Ag). Linear and bent Pt−Fe_3O_4−Ag morphologies account for 15% and 47% of the heterotrimer portion of the product, respectively. Interestingly, the remaining 38% of the heterotrimers appear, at first glance, to consist of Ag−Pt−Fe_3O_4 linkages, with Ag nucleating on the Pt surface. However, HRTEM images, shown and discussed below, confirm that all of the Ag does indeed nucleate on iron oxide, not on Pt.

Figure 5 shows representative HRTEM images for the three types of Pt−Fe_3O_4−Ag heterotrimers that were observed in Figure 4. The linear Pt−Fe_3O_4−Ag heterotrimer exhibits lattice spacings of 2.4, 2.3, and 4.9 Å, which correspond to the (111) plane of Ag, the (111) plane of Pt, and the (111) plane of Fe_3O_4, respectively. The bent Pt−Fe_3O_4−Ag heterotrimer shows lattice spacings of 2.0, 1.9, and 2.5 Å, which are consistent with the (100) plane of Ag, the (100) plane of Pt, and the (311) plane of Fe_3O_4, respectively. The third heterotrimer morphology exhibits lattice spacings of 2.3, 2.3, and 2.9 Å, which correspond to the (111) plane of Ag, the (111) plane of Pt, and the (121) plane of Fe_3O_4, respectively. At low magnification, this third heterotrimer morphology appears to include the conventional Ag−Pt−Fe_3O_4 linkage, but the HRTEM image in Figure 5c reveals that it actually contains a thin amorphous region separating the Pt and Ag domains. This is consistent with the presence of the protective iron oxide shell that was formed during the heterodimer synthesis (see Figure 2b,c), and it indicates that Ag can nucleate on both the Fe_3O_4 domain and on the protective shell, since both consist of iron oxide. Therefore, none of the three heterotrimer morphologies formed using the protected Pt domain contain a Pt−Ag interface, which fully distinguishes

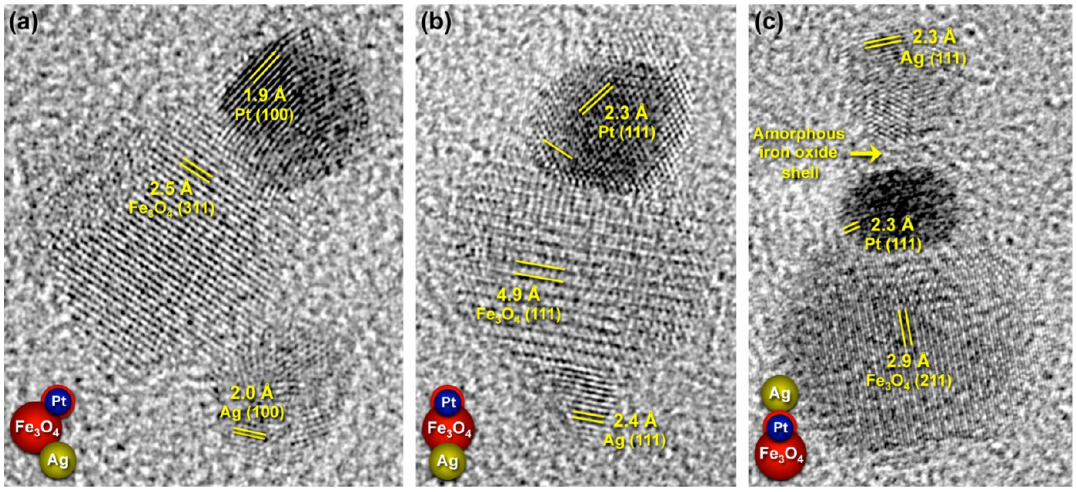

Figure 5. HRTEM images of the three distinct Pt−Fe_3O_4−Ag heterotrimer morphologies that were observed: (a) bent Pt−Fe_3O_4−Ag geometry, (b) linear Pt−Fe_3O_4−Ag geometry, and (c) linear Ag-(FeO_x)−Pt−Fe_3O_4 geometry. In (c), note the region between the crystalline Ag and Pt domains, which corresponds to the amorphous iron oxide shell that surrounds the Pt domain. All three HRTEM images include lattice spacings that are characteristic of Ag, Pt, and Fe_3O_4.

them from the Ag−Pt−Fe_3O_4 configuration that contains exclusively Pt−Ag (and not Ag−Fe_3O_4) interfaces.

Different domain configurations are expected to result in different properties. For reasons outlined previously, Ag−Pt−Fe_3O_4 and Pt−Fe_3O_4−Ag were chosen as model systems for demonstrating the concept of using solid-state protection to direct site-specific nucleation, for accessing multiple distinct ternary nanoparticle isomers, and for understanding how the nanoparticle protecting group chemistry can be reproducibly applied. However, Ag−Pt−Fe_3O_4 and Pt−Fe_3O_4−Ag contain functional domains, including plasmonic Ag nanoparticles, so it is possible to validate that different properties arise from the different configurations. Accordingly, Figure S1 shows UV−visible absorption spectra for Ag−Pt−Fe_3O_4 and Pt−Fe_3O_4−Ag heterotrimers in hexanes. The Pt−Fe_3O_4−Ag sample has a single absorption peak with $\lambda_{max} = 402$ nm, which is consistent with the peak at 400 nm observed for Ag nanoparticles of similar size in hexanes.[30] These results are also consistent with previous studies, which have shown that there is no substantial shift in the plasmon frequency of Ag when it is bound to Fe_3O_4, indicating weak interaction between these domains.[31] In contrast, the Ag−Pt−Fe_3O_4 sample exhibited a single peak at 432 nm, which represents a 30 nm red shift compared to the Pt−Fe_3O_4−Ag isomer and the typical absorption peak for free Ag nanoparticles. The shift in the Ag surface plasmon resonance is likely a result of interaction with the bound Pt domain and is consistent with previous reports describing similar systems. For example, Ag nanoparticles coated with a discontinuous Pt shell were found to exhibit a 37 nm red shift from the characteristic plasmonic absorption of Ag nanoparticles (400 nm), which was attributed to the presence of the Pt domain.[32]

Nucleation of Au on Pt−Fe_3O_4 Heterodimers. To further interrogate the ability of the thin iron oxide shell to prevent the Pt domain from serving as a nucleation site for additional metal nanoparticles, we studied the nucleation of Au onto Pt−Fe_3O_4 heterodimers, both with and without an iron oxide shell covering the Pt. Under the conditions used in these experiments—appropriate soluble metal salts, Pt−Fe_3O_4 heterodimers in nonpolar solvents, and a reaction temperature of 60 °C—it is known that Ag nucleates on both Fe_3O_4 and Pt nanoparticles when they are separate from one another, but Au only nucleates on Pt and not on Fe_3O_4. Therefore, upon reaction of the Pt−Fe_3O_4 heterodimers from Figure 1a with $HAuCl_4$, Au−Pt−Fe_3O_4 was the expected product.[21] Consistent with this, exclusive formation of the Au−Pt−Fe_3O_4 heterotrimer was indeed observed. Representative TEM and HRTEM images of these Au−Pt−Fe_3O_4 heterotrimers are shown in Figure 6b and c, and the observed lattice spacings of 2.0, 1.9, and 2.9 Å are consistent with the (200), (100), and (121) planes of Au, Pt, and Fe_3O_4, respectively.

In contrast, for the Pt−Fe_3O_4 heterodimers having the Pt domain protected by a thin iron oxide shell, only iron oxide is exposed, and thus the entire surface should be unreactive toward nucleation of Au. Consistent with this, when the protected Pt−Fe_3O_4 heterodimers from Figure 2 were reacted with $HAuCl_4 \cdot 3H_2O$ in ODE at 60 °C, we saw no evidence of Au growing on Pt−Fe_3O_4. Representative TEM images (Figure 6e) show unaltered Pt−Fe_3O_4 heterodimers and free Au particles, indicating that Au nucleated independently of the Pt−Fe_3O_4 heterodimers. The corresponding HRTEM image (Figure 6f) shows a lattice spacing of 2.4 Å on a representative free particle, and this is consistent with the (111) plane of Au and lattice spacings in the heterodimer particles of 1.9 and 4.8 Å, which are consistent with the (100) and (111) planes of Pt and Fe_3O_4, respectively.

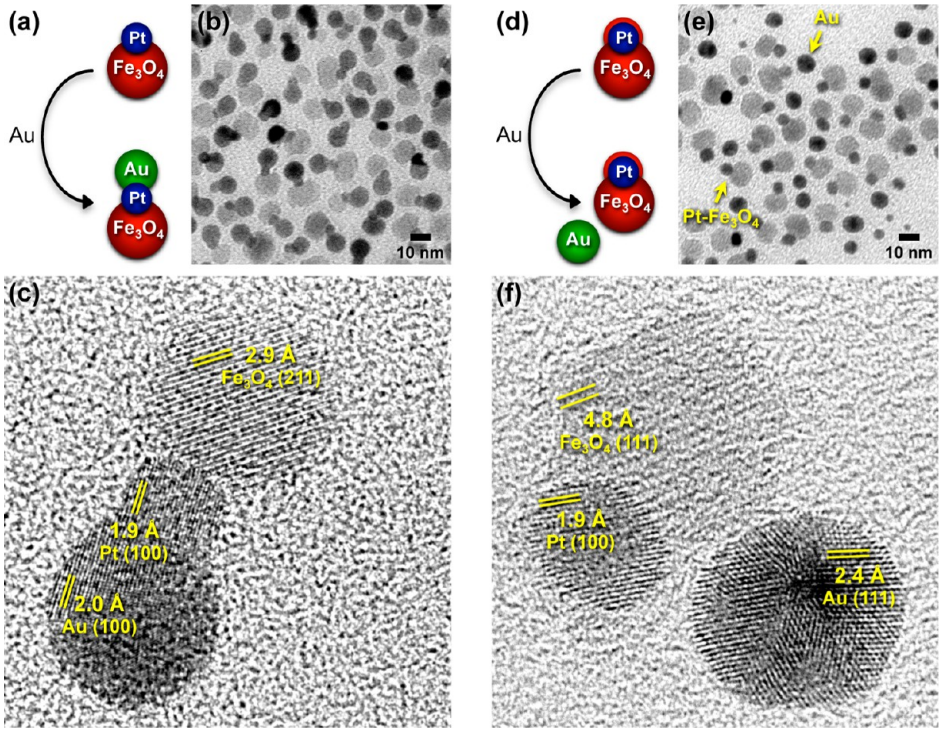

Figure 6. (a) Schematic highlighting the nucleation of Au on Pt−Fe_3O_4 heterodimers (without an iron oxide shell) to form the Au−Pt−Fe_3O_4 heterotrimer and (b) the corresponding TEM image, along with (c) an HRTEM image of a representative Au−Pt−Fe_3O_4 heterotrimer. (d) Schematic highlighting the inability of the protected Pt−Fe_3O_4 heterodimer to nucleate Au and (e) the corresponding TEM image showing free Au particles along with Pt−Fe_3O_4, as well as (f) a representative HRTEM image showing an unbound Au nanoparticle next to a Pt−Fe_3O_4 heterodimer. All HRTEM images exhibit lattice spacings that are characteristic of Au, Pt, and Fe_3O_4.

Understanding and Controlling the Formation of the Iron Oxide Shell. The iron oxide shell that covers the Pt domain of Pt−Fe_3O_4 heterodimers serves as a solid-state analogue of a molecular projecting group, since it prevents Ag and Au from nucleating on the Pt surface, which otherwise would be the most favorable site. Because of the critical role that the iron oxide shell plays in directing the nucleation of the third nanoparticle domain, and therefore in the selective formation of two distinct ternary nanoparticle isomers, it is important to understand how it forms and how it can be controlled. To achieve such understanding, we systematically varied the amount of oleic acid used to synthesize the Pt−Fe_3O_4 heterodimers while keeping the concentrations of $Fe(CO)_5$ and the Pt seeds constant. As mentioned previously, the iron oxide shell coating the Pt domain emerges when the molar ratio of oleic acid to $Fe(CO)_5$ is decreased to 1.5:1 from the standard literature value of 3:1,[29] and therefore oleic acid concentration was identified as the key variable that determines whether or not a protective iron oxide shell forms.

The standard 3:1 molar ratio of oleic acid to $Fe(CO)_5$ is the precise quantity required to form the iron oleate complex $Fe(C_{18}H_{33}O_2)_3$, which is the most likely *in situ* precursor that leads to the formation of the Fe_3O_4 domain. Indeed, when a 3:1 ratio of oleic acid to $Fe(CO)_5$ was used in the synthesis of Pt−Fe_3O_4, the heterodimers showed no visual evidence of an iron oxide shell coating the Pt domain (Figure 7a), and as discussed previously, the Pt domain was clearly exposed because both Au and Ag nucleated on it to form M−Pt−Fe_3O_4 heterotrimers (M = Au, Ag). When the molar ratio of oleic acid to $Fe(CO)_5$ was decreased to 1.5:1—the value used in the preceding sections to protect the Pt domain—the predominant morphology consisted of Pt−Fe_3O_4 heterodimers with a thin iron oxide shell surrounding the Pt domain (Figure 7b). When the molar ratio was decreased further to 0.6:1, an asymmetric core−shell morphology was observed that is best described as a combination of core−shell and heterodimer morphologies (Figure 7c). Finally, when no oleic acid was added to the reaction, the predominant morphology consisted of Pt/iron oxide core/shell and free iron oxide nanoparticles (Figure 7d).

The impact that the molar ratio of oleic acid to $Fe(CO)_5$ has on the morphology of the Pt/Fe_3O_4 nanostructures is clearly visible by comparing the TEM images in Figure 7: as the amount of oleic acid is increased, the morphology can be systematically tuned from a core−shell structure to a heterodimer, and distinct intermediates can be isolated. These observations suggest that there are two competing pathways: one that results in a core−shell structure and one that results in heterodimers. When no oleic acid is present, $Fe(CO)_5$ is the only source of iron, and no iron

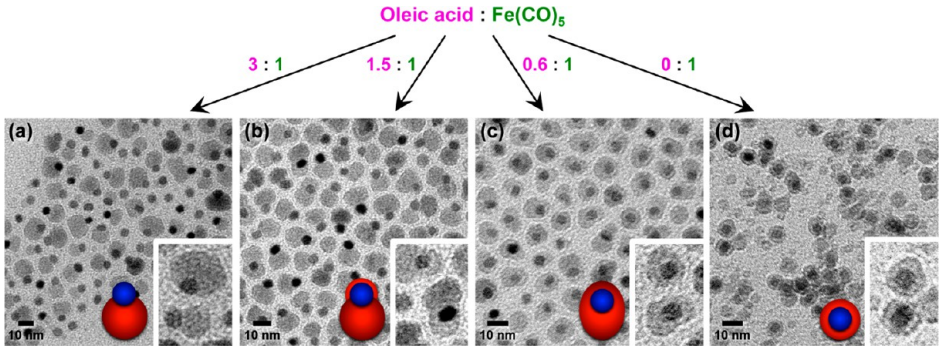

Figure 7. Representative TEM images of iron oxide/platinum nanoparticles formed by varying the ratio of oleic acid to $Fe(CO)_5$ during their synthesis, as indicated: (a) a 3:1 ratio forms Pt−Fe_3O_4 heterodimers, (b) a 1.5:1 ratio forms Pt−Fe_3O_4 heterodimers that have a thin iron oxide shell surrounding the Pt domain, (c) a 0.6:1 ratio forms asymmetric nanostructures that are intermediate between Pt−Fe_3O_4 heterodimers and Pt/Fe_3O_4 core/shell nanoparticles, and (d) no oleic acid forms Pt/Fe_3O_4 core/shell nanoparticles.

oleate can form. $Fe(CO)_5$ is known to thermally decompose in solution to form Fe or Fe alloy nanoparticles,[33] while iron oleate is known to thermally decompose in solution to form iron oxide nanoparticles.[34] We therefore suggest that when only $Fe(CO)_5$ is present, it thermally decomposes in solution to form Fe^0, which deposits onto the surface of the Pt seed particles and oxidizes during workup in air to form a Pt@FeO_x core−shell morphology. In contrast, when sufficient oleic acid is present to react with all of the $Fe(CO)_5$, *e.g.*, at molar ratios ≥3:1, all of the iron in solution exists as iron oleate, which decomposes to produce the Fe_3O_4 domain of the Pt−Fe_3O_4 heterodimers. At intermediate ratios of oleic acid to $Fe(CO)_5$, where oleic acid is the limiting reagent, some of the iron in solution is present as iron oleate, while the rest remains as $Fe(CO)_5$. Therefore, the two competing thermal decomposition reactions can occur simultaneously, and the amount of iron incorporated into the iron oxide shell and the Fe_3O_4 domain is determined by the *in situ* concentration of $Fe(CO)_5$ and iron oleate, respectively. These insights lead to a highly reproducible route for installing the iron oxide protecting group onto the Pt domain.

CONCLUSIONS

A fundamental challenge in the synthesis of high-order hybrid nanoparticles—one that underpins the construction of functional nanoarchitectures for applications that include solar energy conversion and optics—is the controlled placement of one nanoparticle relative to others. Such control is necessary to ensure that the spatial arrangements, domain configurations, and proper materials linkages and interfaces required for a target function can be realized experimentally and in high yield. As an important step toward this goal, we have introduced a solid-state analogue of molecular protecting group chemistry to direct the nucleation of a nanoparticle selectively onto one domain of a colloidal heterodimer *vs* another, effectively rendering the preferred nucleation site inaccessible so that an otherwise disfavored ternary configuration is accessible.

Specifically, we demonstrated that a thin shell of amorphous iron oxide can be installed onto the Pt domain of Pt−Fe_3O_4 heterodimers. Nucleation of Ag onto Pt−Fe_3O_4 typically results in the exclusive formation of Ag−Pt−Fe_3O_4 heterotrimers. However, nucleation of Ag onto Pt−Fe_3O_4 heterodimers that have the Pt domain protected with a thin iron oxide shell instead occurs exclusively on the exposed iron oxide surface, *not* on the Pt. This results in the formation of the otherwise disfavored heterotrimer Pt−Fe_3O_4−Ag, which has a different configuration with distinct materials linkages and also different optical properties than the favored Ag−Pt−Fe_3O_4 heterotrimer. Pt−Fe_3O_4−Ag and Ag−Pt−Fe_3O_4 can be considered as isomers, since they contain the same nanoparticles in different configurations, and therefore the nanoparticle protecting group chemistry provides a predictable pathway to distinct ternary nanoparticle isomers. Such ternary colloidal nanoparticle isomers represent an important step toward controlling the high-order configurations and materials linkages that underpin many emerging applications of colloidal hybrid nanoparticles. Systematic studies revealed that the ratio of oleic acid to $Fe(CO)_5$ used during the synthesis of the Pt−Fe_3O_4 heterodimers is the key variable that controls whether or not a protective iron oxide shell is installed on the Pt domain. These same systematic studies also provided new insights into how one can tune between core−shell and heterodimer morphologies within the same materials system.

This protecting group chemistry represents an important addition to the growing "total synthesis" toolbox for rationally constructing high-order hybrid nanoparticles.[21,27] As a model proof-of-concept system, installing an amorphous iron oxide shell onto the Pt domain of Pt−Fe_3O_4 heterodimers and using it to direct the subsequent nucleation of Ag and Au nanoparticles into otherwise disfavored configurations serves as an initial demonstration of the concept of colloidal nanoparticle protecting group chemistry. However, such protecting group capabilities must be

expanded to other materials systems, be made more selective with respect to subsequent nucleation, and be capable of being removed to re-expose the protected domain. Research along these lines is currently under way. Preliminary evidence suggests that the amorphous iron oxide shell can be removed; thus deprotection is indeed likely to be achievable in this system.

MATERIALS AND METHODS

Materials. 1-Octadecene [ODE, technical grade, 90%], oleic acid [OLAC, technical grade, 90%], platinum(II) acetylacetonate [$Pt(acac)_2$, 97%], iron(0) pentacarbonyl [$Fe(CO)_5$, >99.99%], and gold(III) chloride hydrate [$HAuCl_4 \cdot 3H_2O$] were purchased from Sigma-Aldrich. Silver(I) acetate [$Ag(C_2H_3O_2)$, anhydrous] was purchased from Alfa Aesar. Oleylamine [OLAM, C_{18} content 80–90%] was purchased from Acros Organics. Solvents, including hexanes, toluene, isopropyl alcohol [IPA], and ethanol [EtOH], were of analytical grade. All chemicals were used as received.

Synthesis of 4 nm Pt Nanoparticles. Using a modification of a published procedure,[28] $Pt(acac)_2$ (200 mg) was added to a mixture of 1-octadecene (20 mL), oleylamine (2 mL), and oleic acid (2 mL) in a 100 mL three-neck flask. The solution was heated to 120 °C under vacuum, then heated to 185 °C under a blanket of Ar, at which point 0.2 mL of an $Fe(CO)_5$ solution [0.1 mL of $Fe(CO)_5$ in 1 mL of hexanes] was swiftly injected. The reaction was then heated to 190 °C and left for 1 h. After cooling to room temperature, the particles were precipitated from solution using IPA, followed by centrifugation. The particles were redispersed in hexanes, and the process was repeated using EtOH. The resulting product was suspended in 4 mL of hexanes solution that contained 1% oleylamine and 1% oleic acid.

Synthesis of Pt–Fe_3O_4 Heterodimers. Using a modification of a published procedure,[28] 1-octadecene (10 mL) and oleic acid (0.6 mL) were placed into a 100 mL three-neck flask equipped with a reflux condenser, and the solution was degassed at 120 °C for 30 min under a flow of Ar. The reaction was then placed under an Ar blanket, and $Fe(CO)_5$ [0.07 mL dispersed in 0.25 mL of ODE] was injected. After 5 min, oleylamine (0.5 mL) and then Pt seeds [10 mg in 1 mL of hexanes dispersion] were injected. The reaction was heated to 310 °C and left for 30 min. After cooling to room temperature, the particles were precipitated from the cooled solution using IPA, followed by centrifugation. The particles were then redispersed in hexanes, and the process was repeated using EtOH. The resulting product was suspended in 4 mL of hexanes solution that contained 1% oleic acid and 1% oleylamine.

Synthesis of Pt–Fe_3O_4 Heterodimers with an Iron Oxide Shell. Pt–Fe_3O_4 heterodimers with an iron oxide shell on the Pt domain were synthesized using the same procedure described above except that the volume of oleic acid was decreased to 0.25 mL. The volume of oleic acid was further decreased to 0.1 and 0 mL to increase the thickness of the shell.

Synthesis of Ag–Pt–Fe_3O_4 and Pt–Fe_3O_4–Ag Heterotrimer Isomers. $Ag(C_2H_3O_2)$ (12.5 mg) was dissolved in toluene (10 mL) that contained oleylamine (0.75 mL), followed by the addition of Pt–Fe_3O_4 heterodimers (10 mg in 1 mL of hexanes suspension) with or without a shell, depending on which heterotrimer isomer was desired. The solution was heated to 60 °C under an Ar blanket and left for 14 h. After cooling to room temperature, the product was precipitated using EtOH and centrifuged for 3 min at 9000 rpm. The resulting product was suspended in 4 mL of hexanes solution that contained 1% oleic acid and 1% oleylamine.

Au/Pt–Fe_3O_4 Control Experiment. $HAuCl_4 \cdot H_2O$ (25 mg) was dissolved in 1-octadecene (5 mL) and oleylamine (0.75 mL) in a 50 mL flask, and the solution was heated to 60 °C, at which point Pt–Fe_3O_4 heterodimers (10 mg in 1 mL of hexanes) were injected. The temperature was held at 60 °C for 4 h. After cooling to room temperature, the particles were precipitated with IPA, followed by centrifugation. The resulting product was suspended in 4 mL of hexanes solution that contained 1% oleic acid and 1% oleylamine.

Characterization. Transmission electron microscopy (TEM) images were obtained using a JEOL 1200 EX II operating at 80 kV. High-resolution TEM (HRTEM), high angle annular dark-field scanning transmission electron microscopy (HAADF-STEM), and STEM energy-dispersive spectroscopy (STEM-EDS) analyses were obtained using a JEOL 2010F field emission microscope operating at 200 kV and equipped with an EDAX solid-state X-ray detector. ES Vision software (Emispec) was used for EDS data analyses. Particle distributions were determined using ImageJ software. Samples for TEM and STEM-EDS were prepared by drop-casting nanoparticles dispersed in hexanes onto Formvar-coated Cu grids. Lattice spacings were determined using HRTEM images and ImageJ software. UV–visible absorption spectra were acquired on nanoparticles dispersed in hexanes using an Ocean Optics HR400 spectrometer equipped with a DH-2000-BAL light source.

Conflict of Interest: The authors declare no competing financial interest.

Acknowledgment. This work was supported by the U.S. National Science Foundation under grant CHE-1213475. TEM imaging was performed in the Penn State Microscopy and Cytometry Facility (University Park, PA, USA), and HRTEM imaging was performed at the Materials Characterization Lab of the Penn State Materials Research Institute.

Supporting Information Available: UV–visible absorption spectra for Ag–Pt–Fe_3O_4 and Pt–Fe_3O_4–Ag heterotrimers. This material is available free of charge *via* the Internet at http://pubs.acs.org.

REFERENCES AND NOTES

1. Carbone, L.; Cozzoli, P. D. Colloidal Heterostructured Nanocrystals: Synthesis and Growth Mechanisms. *Nano Today* **2010**, *5*, 449–493.
2. Costi, R.; Saunders, A. E.; Banin, U. Colloidal Hybrid Nanostructures: A New Type of Functional Materials. *Angew. Chem., Int. Ed.* **2010**, *49*, 4878–4897.
3. Cozzoli, P. D.; Pellegrino, T.; Manna, L. Synthesis, Properties and Perspectives of Hybrid Nanocrystal Structures. *Chem. Soc. Rev.* **2006**, *35*, 1195–1208.
4. Wang, C.; Xu, C.; Zeng, H.; Sun, S. Recent Progress in Synthesis and Applications of Dumbbell-Like Nanoparticles. *Adv. Mater.* **2009**, *21*, 3045–3052.
5. Casavola, M.; Buonsanti, R.; Caputo, G.; Cozzoli, P. D. Colloidal Strategies for Preparing Oxide-Based Hybrid Nanocrystals. *Eur. J. Inorg. Chem.* **2008**, *6*, 837–854.
6. Mieszawska, A. J.; Jalilian, R.; Sumanasekera, G. U.; Zamborini, F. P. The Synthesis and Fabrication of One-Dimensional Nanoscale Heterojunctions. *Small* **2007**, *3*, 722–756.
7. Hu, J.; Bando, Y.; Golberg, D. Novel Semiconducting Nanowire Heterostructures: Synthesis, Properties and Applications. *J. Mater. Chem.* **2009**, *19*, 330–343.
8. Feng, X.; Hu, G.; Hu, J. Solution-Phase Synthesis of Metal and/or Semiconductor Homojunction/Heterojunction Nanomaterials. *Nanoscale* **2011**, *3*, 2099–2117.
9. Chaundhuri, R. G.; Paria, S. Core/Shell Nanoparticles: Classes, Properties, Synthesis Mechanisms, Characterization, and Applications. *Chem. Rev.* **2012**, *112*, 2373–2433.
10. Amirav, L.; Alivisatos, A. P. Photocatalytic Hydrogen Production with Tunable Nanorod Heterostructures. *J. Phys. Chem. Lett.* **2010**, *1*, 1051–1054.
11. a) Elmalem, E.; Saunders, A. E.; Costi, R.; Salant, A.; Banin, U. Growth of Photocatalytic CdSe-Pt Nanorods and Nanonets.

Adv. Mater. **2008**, *20*, 4312–4317. b) Habas, S. E.; Yang, P.; Mokari, T. Selective Growth of Metal and Binary Metal Tips on CdS Nanorods. *J. Am. Chem. Soc.* **2008**, *130*, 3294–3295.
12. Costi, R.; Saunders, A. E.; Elmalem, E.; Salant, A.; Banin, U. Visible Light-Induced Charge Retention and Photocatalysis with Hybrid CdSe-Au Nanodumbbells. *Nano Lett.* **2008**, *8*, 637–641.
13. Bang, J. H.; Kamat, P. Quantum Dot Sensitized Solar Cells. A Tale of Two Semiconductor Nanocrystals: CdSe and CdTe. *ACS Nano* **2009**, *3*, 1467–1476.
14. Yin, H.; Wang, C.; Zhu, H.; Overbury, S. H.; Sun, S.; Dai, S. Colloidal Deposition Synthesis of Supported Gold Nanocatalysts based on Au-Fe_3O_4 Dumbbell Nanoparticles. *Chem. Commun.* **2008**, 4357–4359.
15. Wang, C.; Daimon, H.; Sun, S. Dumbbell-Like Pt-Fe_3O_4 Nanoparticles and Their Enhanced Catalysis for Oxygen Reduction Reaction. *Nano Lett.* **2009**, *9*, 1493–1496.
16. Figuerola, A.; Fiore, A.; Di Corata, R.; Falqui, A.; Giannini, C.; Micotta, E.; Lascialfari, A.; Corti, M.; Cingolani, R.; Pellegrino, T.; *et al.* One-Pot Synthesis and Characterization of Size-Controlled Bimagnetic FePt-Iron Oxide Heterodimer Crystals. *J. Am. Chem. Soc.* **2008**, *130*, 1477–1487.
17. Mokari, T.; Rothenberg, E.; Popov, I.; Costi, R.; Banin, U. Selective Growth of Metal Tips onto Semiconductor Quantum Rods and Tetrapods. *Science* **2004**, *304*, 1787–1790.
18. Xu, C.; Xie, J.; Ho, D.; Wang, C.; Kohler, N.; Walsh, E. G.; Morgan, J. R.; Chin, Y. E.; Sun, S. Au-Fe_3O_4 Dumbbell Nanoparticles as Dual-Functional Probes. *Angew. Chem., Int. Ed.* **2008**, *47*, 173–176.
19. Bradley, M. J.; Biacchi, A. J.; Schaak, R. E. Chemical Transformation of Pt-Fe_3O_4 Colloidal Hybrid Nanoparticles into PtPb-Fe_3O_4 Heterodimers and $(PtPb\text{-}Fe_3O_4)_n$ Nanoflowers. *Chem. Mater.* **2013**, *25*, 1886–1892.
20. Motl, N. E.; Bondi, J. F.; Schaak, R. E. Synthesis of Colloidal Au-Cu_2S Heterodimers via Chemically Triggered Phase Segragation of AuCu Nanoparticles. *Chem. Mater.* **2012**, *24*, 1552–1554.
21. Buck, M. R.; Bondi, J. F.; Schaak, R. E. A Total-Synthesis Framework for the Construction of High-Order Colloidal Hybrid Nanoparticles. *Nat. Chem.* **2012**, *4*, 37–44.
22. Kamat, P. Manipulation of Charge Transfer Across Semiconductor Interface. A Criterion That Cannot Be Ignored in Photocatalyst Design. *J. Phys. Chem. Lett.* **2012**, *3*, 663–672.
23. Fedutik, Y.; Temnov, V.; Woggen, U.; Ustinovich, E.; Artemyev, M. Exciton-Plasmon Interaction in a Composite Metal-Insulator-Semiconductor Nanowire System. *J. Am. Chem. Soc.* **2007**, *129*, 14939–14945.
24. Li, Z.; Wang, L.; Wang, Z.; Liu, X.; Xiong, Y. Modification of $NaYF_4$:Yb, Er@SiO_2 Nanoparticles with Gold Nanocrystals for Tunable Green-to-Red Upconversion Emissions. *J. Phys. Chem. C* **2011**, *115*, 3291–3296.
25. Eustis, S.; El-Sayed, M. A. Why Gold Nanoparticles Are More Precious Than Pretty Gold: Noble Metal Surface Plasmon Resonance and Its Enhancement of the Radiative and Nonradiative Properties of Nanocrystals of Different Shapes. *Chem. Soc. Rev.* **2006**, *35*, 209–217.
26. Park, H.; Choi, W.; Hoffman, R. Effects of the Preparation Method of the Ternary CdS/TiO_2/Pt Hybrid Photocatalysts on Visible Light-Induced Hydrogen Production. *J. Mater. Chem.* **2008**, *18*, 2379–2385.
27. Buck, M. R.; Schaak, R. E. Emerging Strategies for the Total Synthesis of Inorganic Nanostructures. *Angew. Chem., Int. Ed.* **2013**, *52*, 2–27.
28. Wang, C.; Yin, H.; Dai, S.; Sun, S. A General Approach to Noble Metal-Metal Oxide Dumbbell Nanoparticles and Their Catalytic Application for CO Oxidation. *Chem. Mater.* **2010**, *22*, 3277–3282.
29. George, C.; Dorfs, D.; Bertoni, G.; Falqui, A.; Genovese, A.; Pellegrino, T.; Roig, A.; Quarta, A.; Comparelli, R.; Curri, M. L.; *et al.* A Cast-Mold Approach to Iron Oxide and Pt/Iron Oxide Nanocontainers and Nanoparticles with a Reactive Concave Surface. *J. Am. Chem. Soc.* **2011**, *133*, 2205–2217.
30. Liu, S.; Chen, G.; Prasad, P. N.; Swihart, M. T. Synthesis of Monodisperse Au, Ag, and Au-Ag Alloy Nanoaparticles with Tunable Size and Surface Plasmon Resonance Frequency. *Chem. Mater.* **2011**, *23*, 4098–4101.
31. Huang, J.; Sun, Y.; Huang, S.; Yu, K.; Zhao, Q.; Peng, F.; Yu, Hao; Wang, H.; Yang, J. Crystal Engineering and SERS Properties of Ag-Fe_3O_4 Nanohybrids: from Heterodimer to Core-Shell Nanostructures. *J. Mater. Chem.* **2011**, *21*, 17930–17937.
32. Yang, J.; Sargent, E.; Kelley, S.; Ying, J. Y. A General Phase-Transfer Protocol for Metal Ions and its Applications in Nanocrystal Synthesis. *Nat. Mater.* **2009**, *8*, 683–689.
33. Peng, S.; Wang, C.; Xie, J.; Sun, S. Synthesis and Stabilization of Monodisperse Fe Nanoparticles. *J. Am. Chem. Soc.* **2006**, *128*, 10676–10677.
34. Park, J.; An, K.; Hwang, Y.; Park, J.; Noh, H.; Kim, J.; Park, J.; Hwang, N.; Hyeon, T. Ultra-Large-Scale Synthesis of Monodisperse Nanocrystals. *Nat. Mater.* **2004**, *3*, 891–895.